PHYSICAL REVIEW B VOLUME 22, NUMBER 8 15 OCTOBER 1980

Temperature-dependent angle-resolved x-ray photoemission study of the valence bands of single-crystal tungsten: Evidence for direct transitions and phonon effects

Z. Hussain,* C. S. Fadley,† S. Kono, and L. F. Wagner
Department of Chemistry, University of Hawaii, Honolulu, Hawaii 96822
(Received 26 December 1979)

High-resolution angle-resolved x-ray photoemission (XPS) valence-band spectra from a clean W (001) single crystal have been observed to show strong spectral variations both with electron-emission direction and temperature. The spectral changes with direction are in very good agreement with the predictions of a simple direct-transition model assuming free-electron final-state dispersion and constant matrix elements. The effect of photon wave-vector involvement in the wave-vector conservation has also been explicitly observed. The strong temperature dependence noted indicates the importance of phonon-assisted nondirect transitions for Brillouin-zone averaging and demonstrates conclusively the crucial role played by the Debye-Waller factor in the interpretation of photoemission spectra in the XPS regime. Valence-band spectra at various temperatures can, furthermore, be used for isolating the direct and nondirect components in spectra.

I. INTRODUCTION

Following the first observation that angle-resolved x-ray photoemission (XPS) spectra from the valence bands of gold single crystals exhibit pronounced spectral changes with electron-emission direction,[1] such effects have also been noted in single crystals of Ag,[2] Cu,[3,4] Pt,[5] Si,[6] and the layered transition-metal compounds MoS_2 and GaSe.[7] Since final-state band-structure calculations at these high energies are not yet available, substantial approximations are, in general, required for the interpretation of such spectra. Two inherently different limiting models have by now been proposed for interpreting the changes observed in spectra with emission direction in the XPS regime. In the early work by Baird *et al.*,[1] a simple model based upon direct ($\vec{k}$-conserving) transitions between initial electronic states with full bulk translational symmetry and final-states with a free-electron dispersion relation has been utilized. Matrix elements for all transitions are assumed to be constant. In this model, spectral changes arise mainly because different regions of the Brillouin zone (BZ) are sampled for emission along different directions. This direct-transition model has been unambiguously demonstrated to predict most of the spectral changes with photon energy and emission direction for Cu in the intermediate energy range 30–200 eV.[8-12] Although calculations based upon this approach were also initially found to predict qualitatively the spectral changes observed in XPS spectra for certain metals,[1,3] subsequent studies[13,14] have indicated that at these energies a rather complete averaging over the reduced zone occurs. The second model, first proposed by McFeely *et al.*,[2] takes a completely different approach and assumes that complexities in the final-state electronic wave function involving the mixing in of other plane-wave components by the crystal potential, as well as the finite acceptance angle of the analyzer, finally yield complete sampling of all states in the BZ.[2,4,14-16] The final-state mixing may involve both bulk- and surface-scattering processes.[17] Under this assumption, anisotropies in XPS valence-band spectra must arise due to directional matrix elements as summed over all occupied initial states. These matrix elements are, in turn, calculated by assuming a plane-wave final-state wave function.[2,15] The results of this model agree semiquantitatively with certain prior experimental results,[2,4,15] but it has been pointed out as a result of more accurate calculations by Sayers and McFeely[16] and Goldberg, Fadley and Kono[18] that this agreement has most likely been the result of a fortuitous cancellation of errors in determining the matrix elements.

The at-first-sight somewhat contradictory observations of strong direct-transition effects in the intermediate energy range[8-12] from 30 to 200 eV and full zone averaging in the XPS region of $\sim 10^3$ eV for several substances[13,14] has been tentatively explained by Shevchik,[19] who first pointed out the possible importance of phonon-assisted nondirect transitions in the photoemission process. According to this work[19] there are two contributions to the photoemission spectra: one from direct transitions and the other from phonon-assisted nondirect transitions. The relative importance of these two is determined by the Debye-Waller factor, so that the latter effect becomes more significant at high temperatures and/or at high energies of excitation. Most simply, the percentage of transitions that are direct is given by the Debye-Waller factor. The strong tempera-

ture dependence of valence-band spectra expected as a result of such phonon involvement has been verified experimentally in low-energy angle-resolved photoemission ($\hbar\omega \approx 45$ eV) from Cu by Williams *et al.*[10] However, an attempt to observe such effects in the XPS of Au and Pt between 77 and 293 K gave negative results, and led Dabbousi *et al.*[14] to conclude that complexities in the final electronic state were responsible for zone averaging in the XPS regime. Thus, the exact origin of the zone averaging in XPS remained a question.

A principle aim of this work has thus been to determine the mechanism responsible for zone averaging in the XPS regime. A preliminary account of these results appears elsewhere.[20] The system selected for these studies was a W single crystal. This choice is rather unique in the sense that, even at ambient temperature, over half of the transitions in the XPS regime might be expected to be direct. That is, the Debye-Waller factor is ~0.55. Thus, measurements at higher temperatures may exhibit changes due to an increased degree of zone averaging caused by phonon involvement. On the other hand, any zone averaging due to final electronic state complexities[14,16] would be expected to be almost temperature invariant. Our temperature-dependent XPS studies on W do, in fact, strongly suggest that the principal mechanism responsible for BZ averaging is phonon-assisted nondirect transitions. A second goal of the investigation has been to determine the degree to which the simple direct-transition model described previously can be used to predict that component of the spectra considered to be direct.

After presenting the experimental procedure in Sec. II, we describe the essence of the simple direct-transition model and the role of thermal vibrations in producing nondirect transitions in Sec. III. In Sec. IV A we present angle-resolved valence-band spectra at ambient temperature and correlate the results with the simple direct-transition model. Section IV B deals with the temperature dependence of valence spectra and their use for isolating direct and nondirect components in spectra. In Sec. IV C, comparisons to prior work are made. Our conclusions are presented in Sec. V.

II. EXPERIMENTAL PROCEDURE

The measurements were performed on a combined XPS–low-energy-electron diffraction (LEED) system involving a Hewlett-Packard 5950A spectrometer with a special low-noise, high-stability, resistive-strip multichannel detector (Surface Science Laboratories Model No. 539), and monochromatized Al $K\alpha$ radiation (1486.6 eV). A two-axis specimen goniometer permitted rotation of the specimen on two axes with a final accuracy of positioning of $\pm 0.5°$ in both the polar- and azimuthal-emission angles. Polar rotations were performed about an axis perpendicular to the plane containing the directions of x-ray incidence and electron emission, as well as the [001] surface normal. Azimuthal rotations were about the surface normal. The experimental geometry is shown in Fig. 1. The polar angle θ was measured with respect to the surface, such that 90° corresponds to emission perpendicular to the surface. The azimuthal angle ϕ was measured with respect to the [100] crystal direction. The fixed angle of 72° between x-ray incidence and electron emission means that the polarizations in the unpolarized Al $K\alpha$ radiation are averaged in a plane at 18° with respect to the emission direction[21] (that is, a plane passing through $\theta - 18°$). A specially constructed ultra-high-temperature specimen holder which permitted full polar and azimuthal rotations provided temperatures up to 2700 K. The specimen heater consisted of a flat, spirally-wound, tungsten filament positioned behind the single crystal that was used for both radiative heating of the crystal for high-temperature XPS experiments ($\leq$1200 K) and for electron-bombardment heating in cleaning the crystal by flash desorption at ~2600 K. Possible effects due to the magnetic field induced by the direct-current coil were estimated to be less than 0.2 gauss and thus would deflect the electrons by less than 0.2°. The insignificance of the magnetic field as it affected the valence-band spectra was further confirmed by changing the polarity of the

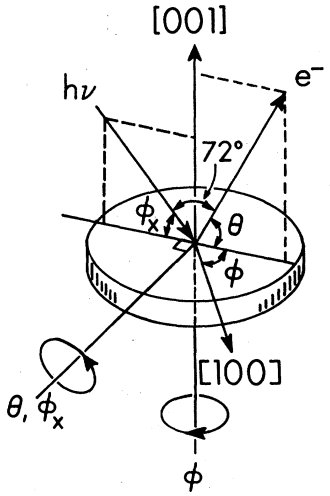

FIG. 1. Schematic illustration of the experimental geometry, with various pertinent angles defined. Rotation of the specimen on both axes noted was possible. The angle between incidence and emission was fixed at 72°.

heater current; this was found not to change *any* spectral features. Temperatures were measured with a theromocouple-calibrated infrared pyrometer (Ircon Model 300LC). Base pressures during measurements were 5×10^{-11} to 1×10^{-10} torr.

A tungsten single crystal with dimensions of 6-mm diameter × 1-mm thickness was oriented to within 0.5° of (001) as checked by the Laue back-reflection method. The crystal was polished using standard mechanical techniques and, just prior to insertion in the ultrahigh-vacuum chamber, it was chemically etched to remove surface disorder introduced by the mechanical polishing. *In situ* cleaning was carried out by high-temperature oxygen exposure (1.0×10^{-7} torr at 2300 K), followed by flashing at 2600 K. Both LEED patterns and final-state diffraction effects in core-peak XPS angular distributions were utilized to verify good surface order and to specify the orientation of the crystal in the system with a precision better than 1°. XPS core spectra were used for monitoring surface contaminants.

Spectra were obtained for various electron-emission directions and, for several directions, also at four different temperatures (295, 500, 700, and 1000 K). For runs at temperatures less than 1000 K, no contaminants were observed either before or after the valence measurements. In runs at 1000 K, the only detectable impurity was ≤ 0.1 monolayer of oxygen, which was found not to affect the reversibility of spectral changes with temperature to within statistical error. Also, in view of the much lower photoelectric cross section for the oxygen valence levels as compared to the W valence levels,[22] as well as the high degree of bulk sensitivity in XPS experiments at relatively high θ values, such impurity levels should have a negligible effect on valence spectra. All of the spectral variations noted with temperature were completely reversible and reproducible. The directions studied included 5°-step azimuthal scans from $\phi=0°$ to 90° for both $\theta=33°$ and $\theta=63.4°$ and 2°-step polar scans for $\phi=0°$ centered about the symmetry-equivalent [102] and [201] directions at $\theta=63.4°$ and 26.6°, respectively. By utilizing two different lens magnifications for the electron spectrometer,[23] it was possible to maintain experimental resolutions always at between 0.7 and 0.8 eV for the W $4f_{7/2}$ core level, even though resolution is in general a function of θ for this spectrometer.[23] Detailed electron-trajectory calculations[23] indicate that the lens accepts electrons in a cone of 3.5° half-angle for the normal mode utilized at low angles of $\theta\approx30°$, and 2.8° for the second mode used at high angles of $\theta\approx60°$. All spectra were accumulated to ~10^4 counts full scale, and the inelastic background at low energies has been subtracted using a previously described, self-consistent method.[24] The data were subsequently smoothed by doing least-squares polynomial fits of second order over nine points or a range of 0.7 eV.[25] No significant spectral features were altered by this smoothing, however. The Fermi level is specified in all spectra with respect to the W $4f_{7/2}$ binding energy, which is taken to be 31.5 eV.[26]

III. THEORY

A. The direct-transition model

In this model, as first proposed by Baird, Wagner, and Fadley[1] for interpreting angle-resolved photoemission spectra in the XPS regime, rigorous wave-vector and energy conservations are required in order for a transition to be allowed. Here, we only briefly summarize this simple model since it has been described in detail in previous studies.[1,3,8,12,13] The energy and wave-vector conservation equations are $E^f=E^i+\hbar\omega$ and $\vec{k}^f=\vec{k}^i+\vec{k}_{\hbar\omega}+\vec{g}$, where E^f and E^i are the final and initial electron energies, $\vec{k}^f$ is the final-state wave vector inside the crystal, $\vec{k}^i$ is the initial-state wave vector, $\hbar\omega$ is the photon energy, $\vec{k}_{\hbar\omega}$ is the photon wave vector (with $|\vec{k}_{\hbar\omega}|=\omega/c$), and $\vec{g}$ is a reciprocal-lattice vector. $\vec{k}^i$ is taken to be inside the reduced Brillouin zone (BZ) so that $E^i(\vec{k}^i)$ is then the band structure of the occupied states, and $\vec{k}^f$ is expressed in an extended-zone scheme. $\vec{k}^f$ is further assumed to correspond to the free-electron dispersion relation $E^f=\hbar^2(k^f)^2/2m$. The photon wave vector $\vec{k}_{\hbar\omega}$ cannot be neglected in the XPS regime where $E^f\approx1.5$ keV, even though it is quite valid to neglect it at ultraviolet energies up to ~100 eV. For example, for the case of Al $K\alpha$ excitation of bcc tungsten with a lattice constant of $a=3.16$ Å, $|\vec{k}_{\hbar\omega}|\approx(0.38)2\pi/a$ and $|\vec{k}^f|\approx(10.1)2\pi/a$, where $2\pi/a$ is the approximate radius of the BZ. Thus $\vec{k}_{\hbar\omega}$ cannot be neglected with respect to $\vec{k}^i$, as $|\vec{k}^i|\lesssim2\pi/a$.

The fact that the spectrometer lens system accepts electrons in relatively narrow, but finite, cones of 3.5° half-angle for the normal mode and 2.8° for the second mode (cf. Fig. 11 in Ref. 23), leads to an additional summation over $\vec{k}^f$ values. That is, the cone accepted by the electron lens permits the observed $\vec{k}^f$ values to lie on an essentially planar disk with a radius of $0.62(2\pi/a)$ or $0.49(2\pi/a)$, respectively, depending on the lens mode use. For each $\vec{k}^f$ value on the disk, since the direction of $\vec{k}_{\hbar\omega}$ is known from the spectrometer geometry, there is a unique value of $\vec{g}$ which, by wave-vector conservation, projects this $\vec{k}^f$ into the reduced BZ to a unique value of $\vec{k}^i$. The corresponding $E^i(\vec{k}^i)$ is found by a second-order Taylor-series interpolation of the relativis-

tic augmented plane-wave (RAPW) band structure given by Christensen and Feuerbacher.[27] Matrix elements are completely neglected in this model, so that each allowed transition is counted with equal weight. A summation is made over a representative set of $\vec{k}^f$ points over the disk. Spectral changes with emission directions are thus connected solely with the *region* of the reduced zone from which transitions are allowed, that is, the projection of the $\vec{k}^f$ disk into the reduced zone. A momentum smearing $\Delta\vec{k}^f$ parallel to $\vec{k}^f$ due to inelastic scattering[11,12] with a mean free path of 13 Å (Ref. 28) is also included in the calculation, although this effect is found to change the calculated curves very little. Such a $\Delta\vec{k}^f$ is rather small in any case, having a magnitude of only $\sim 0.02(2\pi/a)$. The resulting theoretical curves thus obtained are finally broadened with a Gaussian function of 0.8 eV full width at half maximum (FWHM), to simulate the instrumental and natural linewidth contributions. Electron refraction at the surface due to an inner potential of ~16.6 eV (Ref. 27) has also been included in associating $\vec{k}^f$ inside the crystal with the observed $\vec{K}^f$ outside the crystal, although for $\theta \gtrsim 30°$, this effect is essentially negligible.

In conclusion, we stress that this is a very simple, limiting model that certainly does not contain all of the physical ingredients of an exact theory. For example, we refer to the qualitative discussion of mixing in the final states due to bulk and surface scattering by Paasch.[17] Our aim here is thus to investigate the degree to which such an easily visualized and used model can predict certain trends in the experimental data, and thus also provide some guidance in the development of more exact theoretical treatments for the XPS regime.

B. Thermal disorder and nondirect transitions in x-ray photoemission

Shevchik[19] has recently pointed out the effects of thermal disorder in destroying $\vec{k}$ conservation in photoemission and that this phenomenon becomes extremely important for most materials at room temperature in the XPS regime. The temperature dependence of the intensity of radiation elastically scattered by a crystal lattice is commonly estimated in diffraction theory[29] from the Debye-Waller factor,

$$W(T) = \exp[-\tfrac{1}{3}\Delta k^2 \langle U^2(T)\rangle], \tag{1}$$

where $\Delta\vec{k} = \vec{k}^f - (\vec{k}^i + \vec{k}_{\hbar\omega}) = \vec{g}$ = the wave-vector change associated with the scattering and $\langle U^2(T)\rangle$ is the temperature-dependent mean-squared atomic displacement. In a simple one-electron picture, angle-resolved photoemission can be visualized as a diffraction process in which an initial state involving photon momentum $\vec{k}_{\hbar\omega}$ and a bound valence-electron state of crystal momentum $\vec{k}^i$ is the incident beam, and a final state of momentum $\vec{k}^f$ is the scattered beam. In contrast to usual diffraction theory,[29] the magnitude of the momenta in the initial and final states are different in photoemission. Nonetheless, the diffraction law $\vec{k}^f - (\vec{k}^i + \vec{k}_{\hbar\omega}) = \vec{g}$ describing elastic scattering by a crystal lattice also describes the direct-transition requirement in photoemission. Hence, the intensity of a direct-transition peak should be expected to exhibit a *temperature* dependence in accordance with Eq. (1), as well as a dependence on *energy* due to the change in $\Delta\vec{k} = \vec{g}$ with changing $\hbar\omega$. In addition, the nondirect (phonon-assisted) transition process in photoemission should correspond closely to x-ray or electron thermal diffuse scattering.[29] The temperature dependence of the photoemission can then be estimated by employing simple Debye theory,[29] in which it is assumed that the atoms move independently of one another. In this approximation, the probability that an initial state of momentum $\vec{k}^i$ makes a transition into a final state of momentum $\vec{k}^f$ is proportional to

$$\sigma^{if}(\vec{k}^f)\left([1 - W(T)] + W(T)\sum_{\vec{g}} \delta(\Delta\vec{k} - \vec{g})\right). \tag{2}$$

Here, $\sigma^{if}(\vec{k}^f)$ is the photoionization cross section. The second term in Eq. (2) corresponds to $\vec{k}$-conserving transitions as multiplied by the Debye-Waller factor. The first term in the above expression, however, has no restriction on momentum conservation and thus it corresponds to nondirect transitions. A more detailed analysis of the theory[16,19] shows that phonons provide the source of momentum which could allow all electronic states in the first BZ to contribute to emission into a final state of momentum $\vec{k}^f$. Yet the phonon energy is only a few tens of millivolts, so that it does not seriously alter the energy of the electronic transition. One question that is not addressed is the degree to which phonon-assisted transitions may nonetheless be associated with rather small phonon wave vectors, and thus be quasi direct. For example, it is well known that the thermal diffuse scattering intensity in diffraction is peaked near the Bragg or direct peak.[29] This potential importance of small phonon wave vectors has also been discussed by Sayers and Mc Feely,[16] but our results will eventually show that the rather sharp decomposition of Eq. (2) seems nonetheless to be a very good approximation in XPS.

In the XPS regime, where the momentum of the photoelectron is large, the fraction of direct transitions is expected to be less because of the large $\vec{g}$ and resultant lower value for the Debye-Waller factor for most materials at ambient tem-

perature. The magnitude of the thermal displacements $\langle U^2(T)\rangle$ and the Debye-Waller factors $W(T)$ at four different temperatures [4 K (liquid He), 77 K (liquid N_2), 300 K, and 1000 K] for several elements in the XPS regime ($E_{kin}=1482$ eV), are given in Table I. For most of the commonly studied metals such as Cu, Ag, and Au, the photoemission spectra should be heavily dominated by phonon-assisted nondirect transitions at ambient temperature, although at very low temperatures some restoration of the direct transitions are predicted. Inspection of the table shows that W is a rather unique metal which has a large Debye-Waller factor of 0.55 even at ambient temperature and which *also* exhibits significant variations in the values of $W(T)$ with a change of temperature. Thus, over half of the transitions from W might be expected to be direct at ambient temperature, and measurements at higher temperatures might exhibit changes due to an increased degree of phonon-induced zone averaging.

In comparing experimental spectra obtained at a particular temperature with direct-transition theory, it is thus necessary to take into account phonon-assisted nondirect-transition effects. In doing this, our first set of theoretical curves were generated as follows: The intensities as predicted by the pure direct-transition model $[I_{PDT}(E)]$ were multiplied by $W(T)$ and added to the total density of states $[I_{DOS}(E)]$ after the latter had been weighted

TABLE I. Tabulation of thermal displacements ($\langle U^2\rangle$) and Debye-Waller factors $[W(T)=\exp(-\frac{1}{3}\langle U^2\rangle g^2)]$ in the XPS regime ($E_{kin}=1482$ eV) for various elements. The Debye temperatures are taken from Ref. 30. The solid line divides the Debye-Waller factors so as to indicate when $\geq\frac{1}{2}$ of the transitions will be direct. Elements are in order of Z.

			$T=4$ K		$T=77$ K		$T=300$ K		$T=1000$ K	
Element	Θ_D (K)	A (amu)	$\langle U^2\rangle$ (10^{-18} cm^2)	W	$\langle U^2\rangle$ (10^{-18} cm^2)	W	$\langle U^2\rangle$ (10^{-18} cm^2)	W	$\langle U^2\rangle$ (10^{-18} cm^2)	W
Be	1440	9.012	0.84	0.34	0.86	0.33	1.07	0.25	2.47	0.04
C	2230	12.001	0.41	0.59	0.41	0.59	0.46	0.55	0.83	0.34
Mg	400	24.312	1.12	0.23	1.40	0.16	3.53	0.01		
Al	428	26.981	0.95	0.29	1.15	0.22	2.79	0.03		
Si	645	28.086	0.60	0.46	0.66	0.42	1.26	0.19	3.07	0.02
Ca	230	40.08	1.19	0.21	1.94	0.08	6.24	0.0		
Ti	420	47.9	0.54	0.49	0.66	0.42	1.63	0.12	5.16	0.0
V	380	50.942	0.56	0.48	0.72	0.39	1.85	0.09	5.93	0.0
Cr	630	51.996	0.33	0.65	0.37	0.62	0.71	0.40	2.15	0.06
Mn	410	54.938	0.48	0.53	0.60	0.46	1.49	0.14	4.72	0.0
Fe	470	55.847	0.42	0.58	0.49	0.53	1.13	0.23	3.58	0.01
Co	445	58.933	0.42	0.58	0.50	0.52	1.19	0.21	3.74	0.0
Ni	450	58.71	0.41	0.58	0.49	0.53	1.17	0.22	3.67	0.01
Cu	343	63.54	0.50	0.52	0.67	0.42	1.82	0.09	5.84	0.0
Zn	327	65.37	0.51	0.51	0.70	0.40	1.92	0.08		
Ge	374	72.59	0.40	0.59	0.51	0.51	1.34	0.17	4.28	0.0
As	282	74.922	0.52	0.51	0.77	0.37	2.25	0.05	7.33	0.0
Zr	291	91.22	0.41	0.59	0.60	0.46	1.74	0.10	5.65	0.0
Nb	275	92.906	0.43	0.57	0.65	0.43	1.90	0.08	6.21	0.0
Mo	450	95.94	0.25	0.72	0.30	0.68	0.71	0.39	2.25	0.05
Ru	600	101.07	0.18	0.78	0.20	0.77	0.40	0.60	1.21	0.21
Rh	480	102.905	0.22	0.75	0.26	0.71	0.59	0.46	1.84	0.09
Pd	274	106.4	0.37	0.61	0.57	0.48	1.68	0.11	5.46	0.0
Ag	225	107.87	0.45	0.56	0.75	0.38	2.44	0.04	8.00	0.0
Cd	209	112.40	0.47	0.55	0.81	0.35	2.70	0.03		
Sn	200	118.69	0.46	0.55	0.83	0.34	2.55	0.04		
Sb	211	121.75	0.43	0.57	0.79	0.35	2.46	0.04		
Hf	252	178.49	0.24	0.73	0.39	0.60	1.18	0.22	3.85	0.01
Ta	240	180.948	0.25	0.72	0.42	0.58	1.28	0.19	4.19	0.0
W	400	183.85	0.15	0.82	0.18	0.79	0.47	0.55	1.48	0.14
Re	430	186.2	0.14	0.84	0.17	0.81	0.40	0.59	1.23	0.19
Os	500	190.2	0.11	0.86	0.13	0.84	0.30	0.68	0.92	0.30
Ir	420	192.2	0.14	0.84	0.17	0.81	0.41	0.59	1.29	0.19
Pt	240	195.09	0.23	0.74	0.39	0.60	1.19	0.21	3.88	0.01
Au	165	196.967	0.34	0.65	0.82	0.35	2.46	0.04	8.14	0.0
Pb	105	207.19	0.51	0.52	1.54	0.13	5.75	0.0		

by $[1-W(T)]$:

$$I_{\text{theory}}(E)=[1-W(T)]I_{\text{DOS}}(E)+W(T)I_{\text{PDT}}(E)\,. \quad (3)$$

In these calculations the direct-transition intensities and densities of states were normalized such that the number of points in the first BZ used in calculating the total density of states was taken equal to the number of $\vec{k}^f$ points within the acceptance solid angle (cf. discussion in Sec. IIIA) leading to direct-transition emission. This procedure is approximately equal to normalizing to the same constant area under the two curves $I_{\text{PDT}}(E)$ and $I_{\text{DOS}}(E)$.

IV. RESULTS AND DISCUSSION

A. Ambient-temperature photoemission

Experimental valence-band spectra obtained at ambient temperature for two different azimuthal scans and one polar scan are compared with direct-transition theory as determined by using Eq. (3) in Figs. 2–4. All spectra have been normalized to the same constant maximum height. The experimental spectra in general have four components labeled as 1–4, at ~4.8, ~3.2, ~2.3, and ~0.6 eV, respectively, and the relative intensities of these show changes of varying degree with emission direction. The degree of accuracy in positioning the crystal was also checked for $\theta=33°$ by comparing symmetry-equivalent directions on opposite sides of $\phi=45°$ for $0\leq\phi\leq 90°$. To within statistical error, all spectra showed the correct mirror symmetry about 45°. In general, in Figs. 2–4, there is good qualitative agreement as to the changes predicted and observed in the relative intensities of all four components, as well as in the energy position of peaks 2–4, as discussed in more detail below.

Figures 2 and 3 show comparisons between experiment and theory for spectra obtained in 5°-step azimuthal scans from $\phi=0$ to 45° at $\theta=63.4°$ and $\theta=33°$, respectively. There are marked changes in the relative intensities of all four of the aforementioned components, but especially in peak 1 at ~4.8 eV. For $\theta=63.4°$, this peak shows intensity maxima at $\phi\approx 0°$, 25°, and 45°, and minima at 10°–15° and 35° (Fig. 2), whereas for $\theta=33°$, it shows maxima at $\phi\approx 5°$ and 30°, and minima at 0°, 15°, and 45° (Fig. 3). Figure 5 further indicates the strikingly high degree of agreement between theory and experiment for the intensity changes in this peak. In this figure, the relative intensities of the peak at ~4.8 eV with respect to that at ~2.3 eV are plotted against ϕ for azimuthal scans at both $\theta=63.4°$ and 33°, and *all* of the experimental maxima and minima are correctly predicted by theory. Although theory generally predicts a higher intensity for the 4.8-eV peak than is experimentally observed, this can be attributed mainly to the matrix-element effects that are neglected in this direct-transition model. Checking the location of the initial states contributing to this ~4.8-eV peak in the reduced BZ and inspecting the W band structure[27] show that in all cases these states contain a strong component of plane-

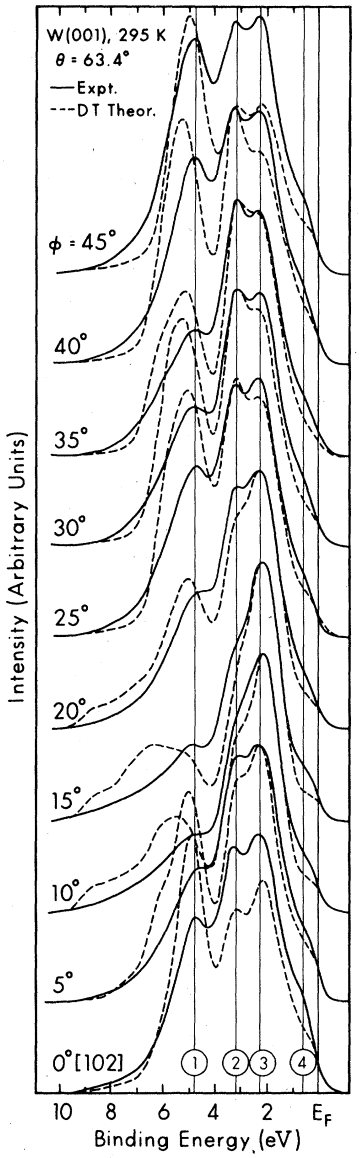

FIG. 2. XPS valence-band spectra obtained in a 5°-step azimuthal scan at $\theta=63.4°$ from $\phi=0°$ to 45° and at ambient temperature (295 K) are compared with direct-transition theory. The theoretical curves are obtained from a weighted sum of the pure direct-transition curves and the density of states, as explained in the text and Eq. (3).

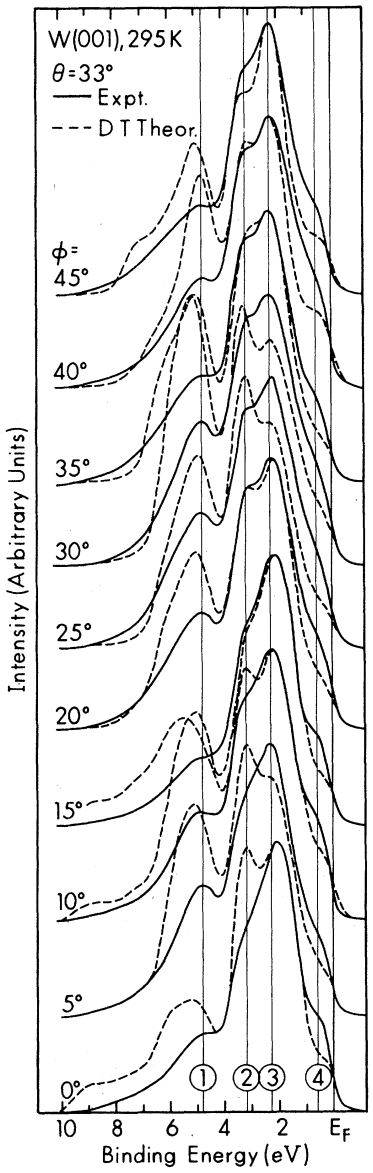

FIG. 3. Same as Fig. 2, except for $\theta = 33°$.

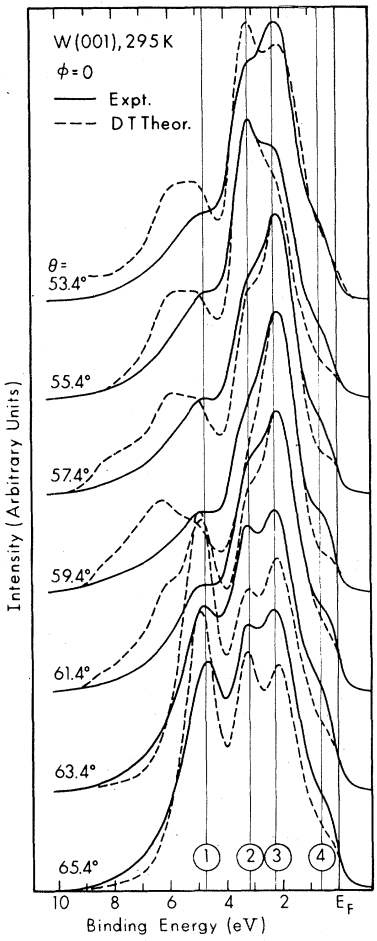

FIG. 4. Same as Fig. 2, but for a 2°-step polar scan at $\phi = 0°$ from $\theta = 53.4°$ to 65.4°.

wave or s-like character. Such character is expected to lead to much smaller matrix elements than the d-like character which is mainly associated with the peaks at 2.3 and 3.2 eV. For example, purely atomic cross-section calculations at XPS energies have been performed for W[31] using the Manson-Cooper central potential model,[32] and these yield a σ_{6s}/σ_{5d} ratio per electron for W of 0.169. Similarly, checking the location of the initial-states contributing intensity to the theoretical spectra for energies $\gtrsim 6$ eV shows that these states arise mainly near the Γ point in the BZ (e.g., the spectra at $\phi = 15°$ in Figs. 2 and 3) and that they contain very strong plane-wave character, thus explaining why they are so strongly suppressed in the experimental results. A further but less obvious, point of agreement between theory and experiment concerns the intensity of the weak shoulderlike emission near ~0.6 eV relative to the peak at ~2.3 eV, which is plotted against ϕ for spectra at $\theta = 63.4°$ and 33° in Fig. 6. Again, the theoretical curves show all of the maxima, minima, and important trends with ϕ of experiment, with the minor exception of a slightly misplaced maximum at $\phi = 25°$, $\theta = 63.4°$. As for components 2 and 3, the theoretical curves are found to be completely consistent with their observed energy positions, even as to certain small energy shifts noted (e.g., of peak 3 for $\phi = 10°$, 15° at $\theta = 63.4°$, and of peak 3 for $\phi = 0°$, 15° at $\theta = 33°$). The degree of agreement between experiment and theory for the relative intensities of these two peaks is also reasonably good, especially for the azimuthal scan at $\theta = 63.4°$, as shown in Fig. 7. The corresponding comparison in Fig. 7 for the azimuthal scan at

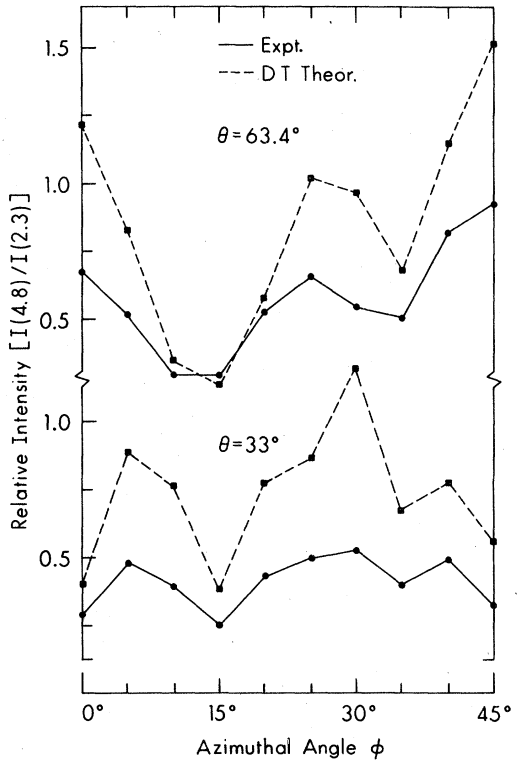

FIG. 5. Azimuthal dependence at 295 K of the intensity of the 4.8-eV peak as measured with respect to that at 2.3 eV for polar angles of 63.4° and 33°. Both experimental values and direct-transition theoretical values according to Eq. (3) are shown.

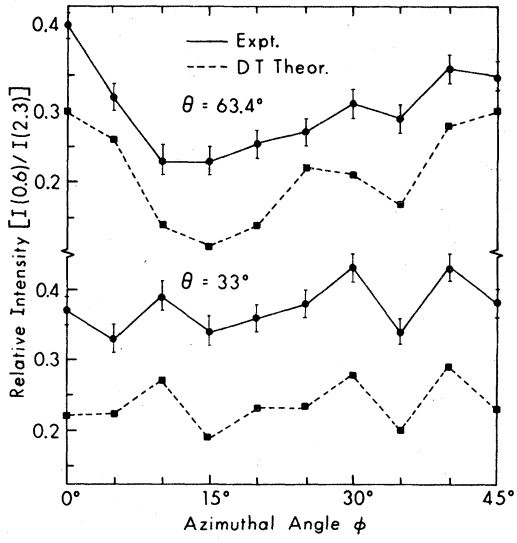

FIG. 6. Same as Fig. 5, except for the intensity of the 0.6-eV shoulder as measured with respect to the peak at 2.3 eV.

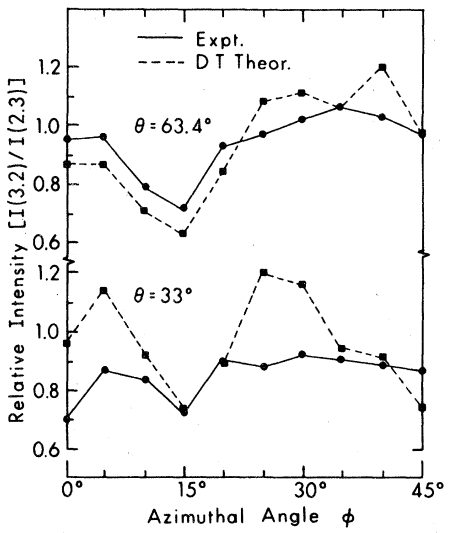

FIG. 7. Same as Fig. 5, except for the intensity of the 3.2-eV peak as measured with respect to the peak at 2.3 eV.

$\theta = 33°$ does not yield quite as good agreement, but theory does exhibit all major maxima and minima.

In Fig. 4, experimental spectra obtained for a 2°-step polar scan from $\theta = 65.4°$ to 53.4° at $\phi = 0°$ are compared with direct-transition theory. In addition to marked changes in the relative intens-

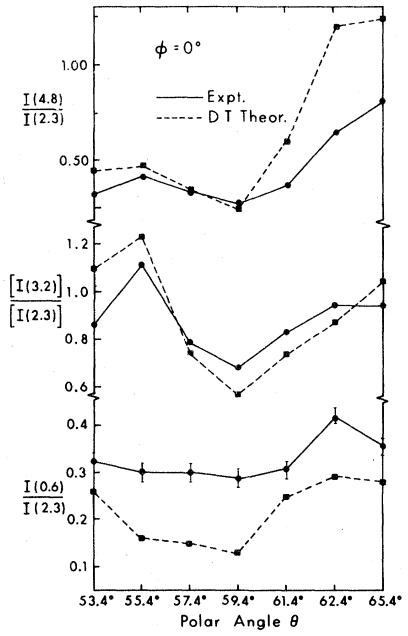

FIG. 8. Polar dependence at 295 K of the intensities of the peaks at 4.8, 3.2, and 0.6 eV as measured with respect to that at 2.3 eV. Both experimental and direct-transition theoretical values according to Eq. (3) are shown.

ity of the peak at ~4.8 eV, very large changes and high sensitivity to emission direction are found for the peak at ~3.2 eV near $\theta = 55°$ that are fully consistent with theory except for a reversal at $\theta = 53.4°$ that is not shown by theory. The degree of accord between experiment and theory for the relative intensities of the components at ~4.8, ~3.2, and ~0.6 eV with respect to that at ~2.3 eV is shown in Fig. 8, and again, all major trends with θ are correctly predicted. The dramatic intensity modulation of the peak at ~3.2 eV with respect to the peak at ~2.3 eV near $\theta = 55°$ is shown in more detail in Fig. 9, where spectra obtained with only 1° steps from $\theta = 57.4°$ to 53.4° are presented. The corresponding theoretical curves are shown only between 1 and 4 eV for simplicity and are directly compared with the experimental data. The theory predicts surprisingly well most of the intensity modulation and high sensitivity of the observed peaks to angle. Although the experimental spectra

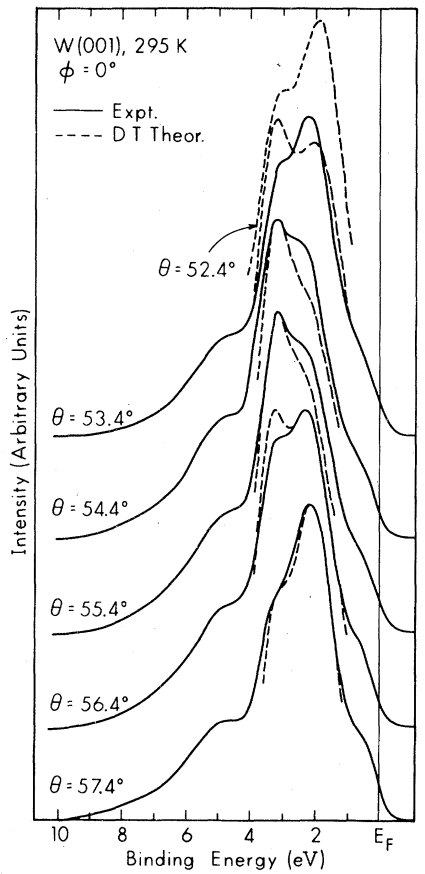

FIG. 9. Valence-band spectra for a fine 1°-step polar scan at $\phi = 0°$ from $\theta = 53.4°$ to 57.4°. Note the strong relative intensity modulation of the peaks at ~3.2 and ~2.3 eV. Direct-transition theoretical spectra are also shown over the energies of ~1–4 eV for comparison.

at both $\theta = 53.4°$ and 56.4° show an ordering of the two itensities that does not agree with theory, it is clear that both theory and experiment are very sensitive to angle changes of as little as 1° (e.g., compare theory at 52.4° with experiment at 53.4°). In view of the $\sim \pm 0.5°$ accuracy of positioning the specimen, such minor discrepancies are thus not surprising. This high sensitivity to emission direction in both experiment and theory also clearly indicates the importance and presence of direct-transition effects, since any changes occurring in matrix elements due to a 1°–2° variation in angle are expected to be relatively small.

In certain cases we have found that a somewhat better degree of agreement between experiment and theory exists for spectra obtained at higher polar angles as compared to those at lower angles (cf. Fig. 7). This could be attributable to surface-specific effects caused by the enhanced surface sensitivity at $\theta \approx 30°$ where the mean emission depth is ~4 atomic layers as compared to that at $\theta \approx 60°$ of ~7 layers. Also, two recent studies[33] have shown that the clean W (001) surface is probably reconstructed at room temperature, an effect which could make surface effects more important than they would otherwise be. Although our LEED measurements gave no significant indications of reconstruction, it is not clear that LEED is very sensitive to this particular structural change.[33] A further point is that LEED measurements indicate that the thermal displacement of the atoms in the first 1–4 layers might be twice as much as that of the bulk.[34,35] This would enhance the effects of thermal disorder, leading to a lower fraction of direct transitions as the surface sensitivity of the photoemission experiment is increased at lower emission angles. However, the degree of agreement we have found between experiment and direct-transition theory for $\theta = 33°$ in Figs. 3, 5, 6, and 7 certainly indicates that surface effects are not strong, even if they are present.

Next, we consider the question of whether one further aspect of direct-transition behavior is observable: the influence of the photon wave vector $\vec{k}_{\hbar\omega}$. At the top of Fig. 10, the predicted effect of $\vec{k}_{\hbar\omega}$ is schematically illustrated. For the geometry of our measurements, this effect is to shift the quantity $\vec{k}^f - \vec{k}_{\hbar\omega} = \vec{k}^i + \vec{g}$ that is directly related to the band structure by 2.0° toward greater θ relative to the exiting direction $\vec{k}^f$. Between the interior and exterior of the surface, $\vec{k}^f$ may also have to be corrected slightly for refraction, although this is only significant for $\theta \leq 30°$. It is now useful to consider polar scans of emission direction near the two-symmetry-equivalent directions [102] at $\theta = 63.4°$, $\phi = 0$ and [201] at $\theta = 26.6°$, $\phi = 0°$, as also illustrated at the top of Fig. 10. If $\vec{k}_{\hbar\omega}$ is

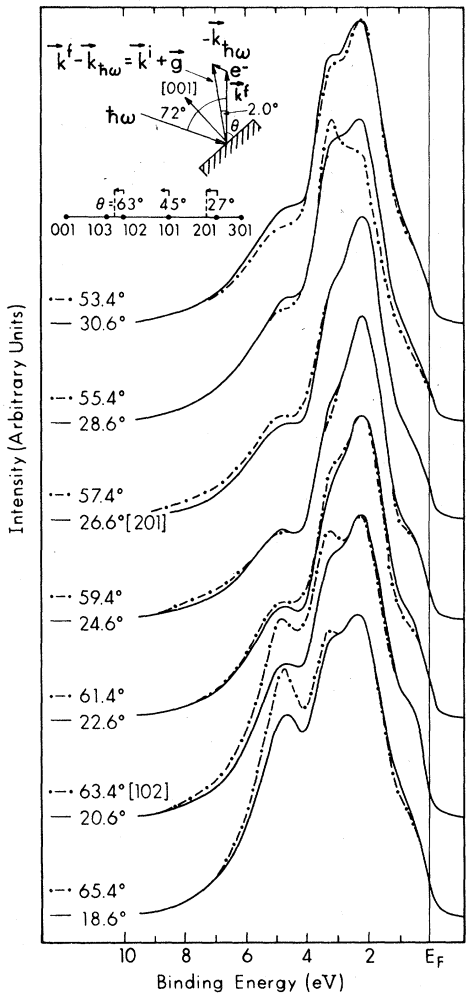

FIG. 10. Effect of photon wave vector $\vec{k}_{\hbar\omega}$ on spectra observed at 295 K for various polar angles near the [102] and [201] directions. The azimuthal angle was 0° for all spectra. The electron-photon geometry is shown, together with the polar-scan range considered and the spectra obtained. In overlaying the spectra, an empirical shift of 6.0° has been added between [102] and [201]. The overall calculated shift due to $\vec{k}_{\hbar\omega}$ and refraction is 4.6°.

important, then emission along [102] will not correspond crystallographically to the same $\vec{k}^i + \vec{g}$ as along [201], but rather to an emission direction at *lower* θ than [201] by $2 \times 2.0°$ plus any refraction correction. Adding in a small refraction correction of ~0.6° that is needed only for θ near [201], one finally predicts a symmetry correspondence in $\vec{k}^i + \vec{g}$ provided that spectra near [201] are shifted to lower θ by 4.6°. Comparison of the two families of spectra centered near [102] and [201] are also shown in Fig. 10. It is empirically found that a shift of 6.0° is needed to obtain the best correspondence of the two sets of spectra. This empirical shift is thus in good agreement with theoretical predictions. By contrast, if one introduces no shift at all (as in comparing, for example, [102] at 63.4° and [201] at 26.6° directly), a very bad correspondence results. We note also that the electron lens system permitted an angular resolution of ±2.8° for spectra obtained at high angles around [102], whereas for the second mode, utilized at lower angles around [201], it had a resolution of ±3.5°.[23] Thus, spectra at lower angles would be expected to be somewhat more smeared due to sampling a disk ~55% larger in the Brillouin zone, and this behavior is found in both experiment and corresponding theoretical calculations that are now shown here. A further point which may assist in explaining certain differences remaining even in the optimally-shifted pairs in Fig. 10 is that this discussion neglects matrix-element effects which will be different even for pairs of spectra with the correct shift because of the different orientation of the polarization averaging in the radiation source relative to the crystal axes (cf. earlier discussion of polarization averaging in Sec. II). That is, polarizations are always averaged in a plane passing through $\theta - 18°$. However, our prior comparisons in Figs. 2–9 make it seem that matrix elements in general represent relatively minor effects. Nonetheless, they could account for some of the slight differences noted between the pairs in Fig. 10 as, for example, between 55.4° and 28.6° and between 63.4° and 20.6°. The spectra around those angle settings have furthermore been found to be extremely sensitive to direction (cf. Fig. 9). Another source of disagreement could also be surface-specific effects due to the enhanced surface sensitivity at $\theta = 20°–30°$ (~3–4 layers mean depth), compared to that at $\theta = 55°–65°$ (~7 layers): For example, the comparisons 63.4°-20.6° and 65.4°-18.6° could be somewhat affected by this. Nonetheless, the generally high degree of agreement present in Fig. 10 permits concluding unambiguously that the effect of photon wave vector can be clearly observed in angle-resolved XPS.

B. Temperature-dependent photoemission

In Figs. 11 and 12 we show experimental spectra obtained at four different temperatures along two different pairs of directions which exhibit both very strong (*and* completely reversible) temperature dependence and very strong sensitivity to emission direction. Figure 11 shows spectra obtained with $\phi = 0°$ along two directions at $\theta = 55.4°$ and 63.4° that are separated by 8° in polar angle, and Fig. 12 shows another pair of spectra at $\theta = 33°$ which are separated by 6° in azimuth. The Debye-Waller factors are indicated for each temperature. In spite of the rather small angle differences be-

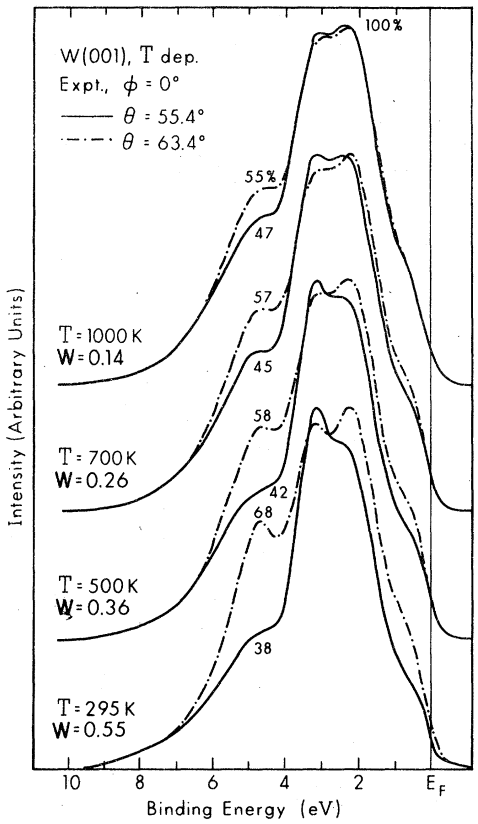

FIG. 11. Temperature dependence of tungsten valence-band spectra for emission at $\phi = 0°$ and $\theta = 55.4°$, 63.4°. The temperatures and their associated Debye-Waller factors are given in the figure, together with the intensity of the peak at 4.8 eV as measured relative to that at 2.3 eV.

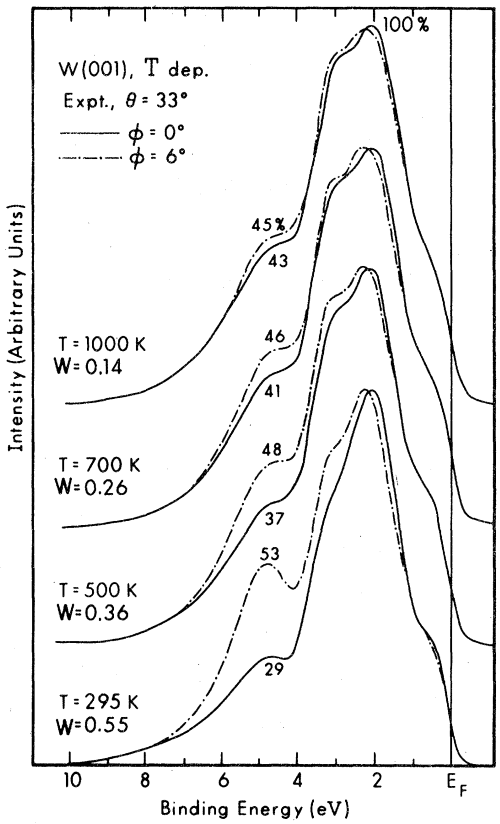

FIG. 12. Same as Fig. 11, except for $\theta = 33°$ along two directions separated by 6° in azimuthal.

tween these two pairs of spectra, all four components of the spectra discussed previously are very different at ambient temperature, especially as regards the relative intensity of the peak at ~4.8 eV in both figures and those at ~0.6, ~2.3, and ~3.2 eV in Fig. 11. However, upon heating the specimen to 1000 K, each pair converges to very nearly the same shape. Note especially the dramatic switching of the relative intensity at ~2.3 and ~3.2 eV in the spectra at $\theta = 55.4°$, and also the marked changes in the relative intensity of the peak at ~4.8 eV in all of the spectra shown. This behavior is thus qualitatively consistent with a strong direct-transition component at lower temperatures and nearly complete BZ averaging at higher temperatures, as variations in spectra with emission direction produced by changing the region of the reduced zone involved in direct transitions would be expected to be more dramatic than matrix-element-associated variations. The slight differences remaining in spectra at high temperatures could be due to both directional matrix elements and to residual direct-transition effects, as $W = 0.14$ at $T = 1000$ K. It might also be asked whether any perturbation in the initial-state band structure is produced by temperature. Knapp *et al.*[36] have recently shown by examining temperature-dependent photoemission studies from copper at much lower energies that observed shifts in the bulk band structure are in agreement with energy shifts calculated for the corresponding temperature-dependent lattice-constant changes. Assuming that this is true also for W, we find that the lattice-constant changes by themselves do not theoretically produce band shifts of much more than ~0.1–0.2 eV.[27] For example, an RAPW calculation with an increase in lattice constant from the value at 300 to 1000 K yields an increase of only ~0.3 eV in the d-band width at the symmetry point H.[27] Thus, it is unlikely that initial-state band-structure changes with temperature represent a significant effect in the spectra of Figs. 11 and 12 that have been observed with the XPS resolution scale of 0.8 eV.

Finally, we consider the validity of separating each spectrum into direct and nondirect components by using temperature-dependent results such

as those in Figs. 11 and 12. That is, we assume that a spectrum at a particular temperature is a sum of a temperature-*in*dependent direct-transition component $[I_{DT}(E)]$ and a temperature-*in*dependent nondirect-transition component $[I_{NDT}(E)]$ weighted by appropriate factors involving the Debye-Waller factor, as

$$I(E,T)=[1-W(T)]I_{NDT}(E)+W(T)I_{DT}(E). \quad (4)$$

Then, since $W(T)$ can be calculated at any temperature, any two spectra at different temperatures T_1 and T_2 can be used to isolate the $I_{DT}(E)$ and $I_{NDT}(E)$. Self-consistency then also requires that the results obtained do not depend on which pair of temperatures are utilized, although, of course, the accuracy will improve as the temperature difference increases.

This method has been applied to temperature-dependent data for 13 distinctly different directions, and it is found to yield a fully self-consistent decomposition into direct and nondirect components. The self-consistency of this procedure is illustrated in Figs. 13 and 14, where direct and nondirect components obtained by using spectra at different pairs of temperatures for emission at $\theta=63.4°$ and $\phi=15°$ and 45° are shown. The two temperatures utilized for isolating each component are also given, along with statistical error bars. For each set of temperature-dependent spectra, the components isolated using different pairs of temperatures are identical within statistical error, thus justifying the validity of this procedure.

A further test of self-consistency can be made by analyzing the temperature-dependent data in a slightly different way in which *all* temperatures are included at once. Namely, Eq. (4) can be rewritten as

$$I(E,T)=[I_{DT}(E)-I_{NDT}(E)]W(T)+I_{NDT}(E). \quad (5)$$

Thus, if the experimental data are adequately described by such an expression, a plot of $I(E,T)$ versus $W(T)$ should yield a straight line of slope $I_{DT}(E)-I_{NDT}(E)$ and intercept $I_{NDT}(E)$. Testing this method of analysis for the spectra involved in Figs. 13 and 14 does indeed yield a straight line, *and* final values of $I_{DT}(E)$ and $I_{NDT}(E)$ that agree com-

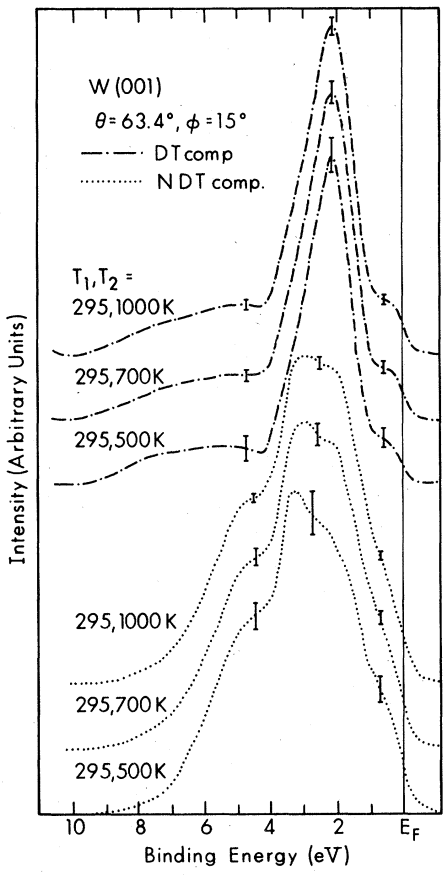

FIG. 13. Direct and nondirect components isolated using various pairs of temperature-dependent spectra obtained at $\theta=63.4°$ and $\phi=15°$. The two temperatures utilized are also given on the curves.

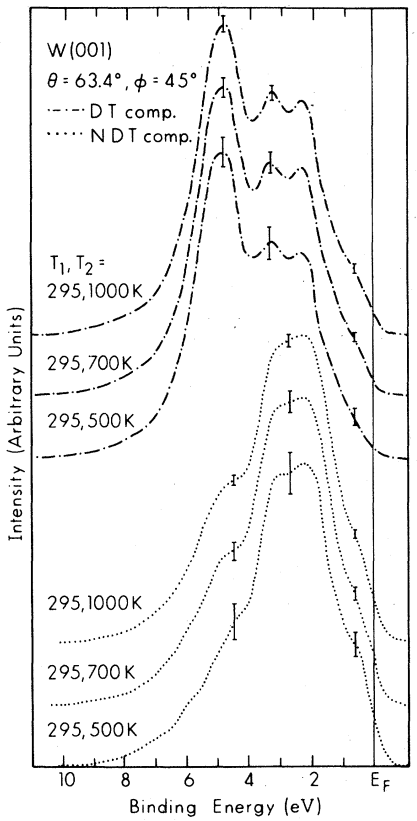

FIG. 14. Same as Fig. 13, except that $\theta=63.4°$ and $\phi=45°$.

pletely with those obtained using the two-temperature analysis based on Eq. (4).

Examples of the final results of this decomposition into direct and nondirect components are shown in Figs. 15 and 16 for eight selected spectra obtained along different directions at higher and lower polar angles, along with ambient-temperature spectra and curves predicted by a *pure* direct-transition model without any density-of-states component. The ambient-temperature spectra and their associated direct-transition components are found to show very high sensitivity to emission direction, as discussed before. The nondirect-transition components, by contrast, are not found to change significantly in these spectra, although some rather subtle changes are seen. The direct-transition components can also be compared directly with curves obtained from the pure direct-transition-model calculations. This comparison shows an improved agreement over comparing theory with the total experimental spectrum, again confirming the validity of such a decomposition. The corresponding comparisons of a mixed direct and nondirect theory with experiment as in Figs.

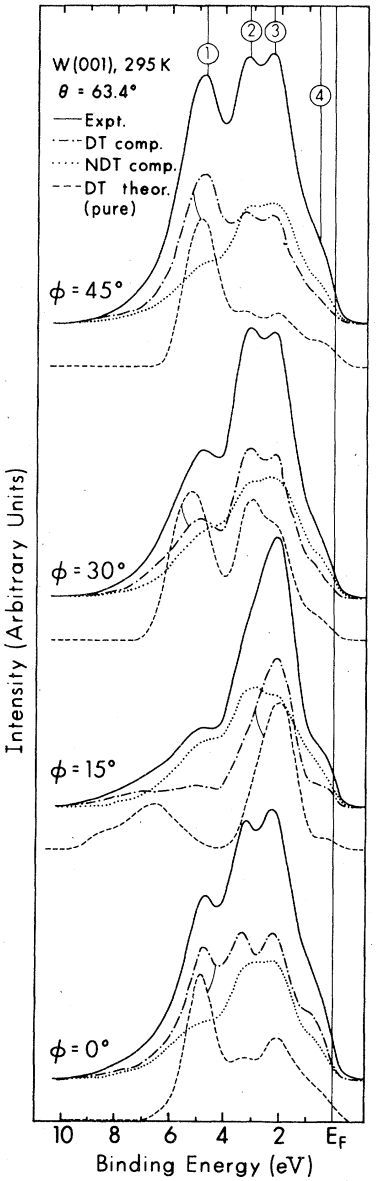

FIG. 15. Experimental spectra obtained at 295 K and $\theta = 63.4°$ for various azimuthal angles ($\phi = 0°$, 15°, 30°, and 45°) are compared with the results of pure direct-transition model calculations. Also shown are the direct and nondirect components of each spectrum as derived from temperature-dependent spectra along each direction. Lines connect the direct component and pure DT theory that should be most directly comparable.

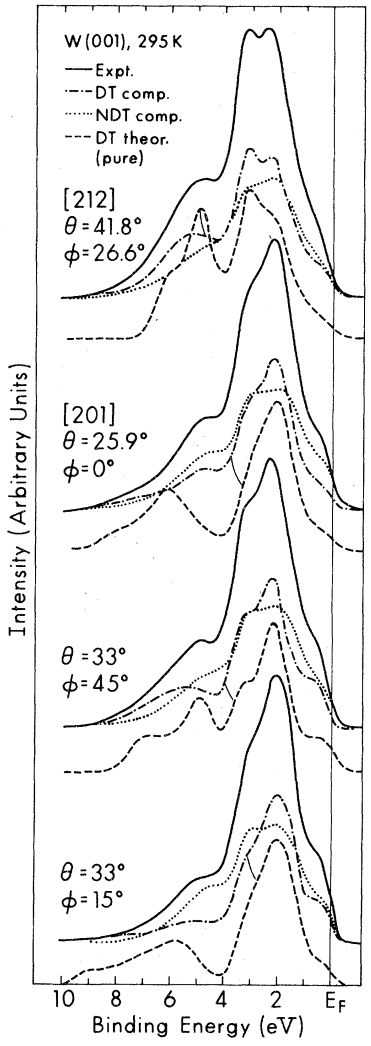

FIG. 16. Same as Fig. 15, but for four different directions at various polar angles lower than those in Fig. 15.

2 and 3 are not as good as those in Figs. 15 and 16. Once again, we should recall that states contributing intensity to theoretical spectra at $\gtrsim$6 eV contain strong plane-wave character and thus are not expected to be observed with full strength due to matrix-element effects.

Having seen various convincing manifestations of direct-transition effects in the XPS of W and also having derived a method for isolating the direct-transition component in purer form, we can now finally ask how directly the observed and predicted spectral changes can be related to the W band structure. Although the disk of $\vec{k}^f$ points sampled in general projects back to a complex surface in the reduced zone, we can estimate which zone regions along high-symmetry directions are the most important in the spectra by looking for points lying close to or on the directions. Specifically, for the 29 equally-spaced points we have used on the disk, we have selected any point which projects back to within $0.05(2\pi/a)$ of a high-symmetry direction. Continuity then implies that there are other points also not very far away. Generally, only 3–5 points satisfying this criterion were found for a given choice of experimental emission direction. An example of such an analysis is shown in Fig. 17 for $\theta = 63.4°$ and $\phi = 0°$, 15°, 30°, and 45°, where the vertical dotted lines on the W band structure indicate $\vec{k}^i$ values for allowed transitions and the horizontal lines indicate the energy locations of the observed spectral features for comparison. Comparing the observed spectra (especially the direct-transition component and pure direct-transition theoretical spectra of Fig. 15) with Fig. 17, we can then see certain connections. For example, peak 1 at 4.8 eV is of maximum relative importance for $\phi = 0°$ and 45°, and Fig. 17 shows that, for these angles, transitions are allowed from relatively flat Δ and G regions in the band structure at ~4.8 eV. This 4.8-eV peak shifts to higher binding energy in theory and decreases in intensity for both experiment and theory in the curves at $\phi = 15°$, and this also is consistent with Fig. 17 where the only allowed transitions are from deeper-lying, very free-electron-like levels that would be expected to have very low relative excitation cross sections. The importance of peak 3 at ~2.3 eV for $\phi = 15°$, as well as a slight shift of it to lower binding energies, is also consistent with allowed transitions from Δ- and Σ-type levels shown in Fig. 17. Thus, although the full 29-point situation is more complex than this, both experiment and theory do qualitatively mirror in a rather direct way the high-symmetry bands shown in Fig. 17. Future experiments with lower temperatures and higher angular resolutions should further enhance the directness of such correlations, perhaps leading to a rather direct method for band-structure mapping with limited complications due to final-state complexity or matrix-element effects.

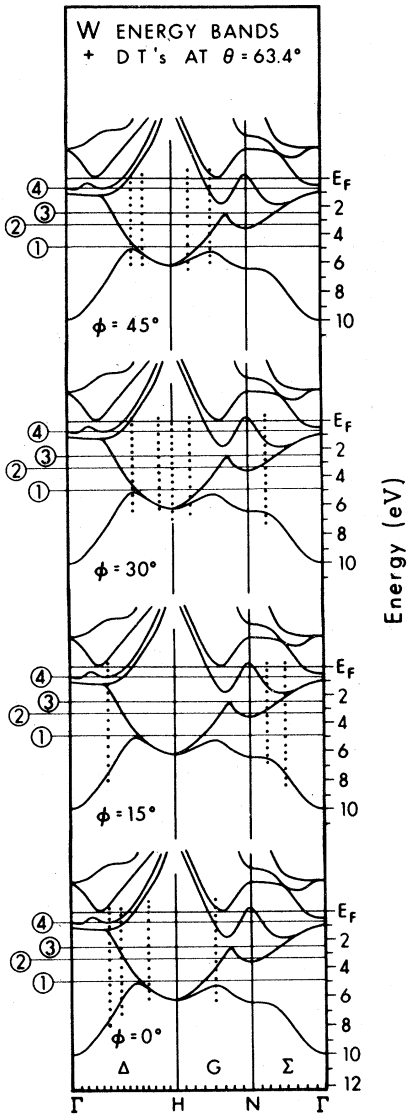

FIG. 17. W band structure along symmetry directions, with the dotted lines showing the $\vec{k}^i$ values of allowed transitions for spectra obtained at $\theta = 63.4°$ and $\phi = 0°$, 15°, 30°, and 45°. The solid lines represent the position of the four observed spectral features in energy. The $\vec{k}^i$ values have been determined as explained in the text.

C. Relationship to prior work

There are two prior studies that warrant discussion in relationship to the present work in that they have reached conclusions that are, at first sight, at variance with those here:

(1) Dabbousi *et al.*[14] have carried out a similar

temperature-dependent study of Au and Pt, working between ambient temperature and liquid-nitrogen temperature, although the specimen temperatures were not measured directly. They observed essentially no changes between high- and low-temperature spectra obtained with emission along the [111] and [100] directions of Au and the [100] direction of Pt and, after comparing their results with the degree of change predicted by a model similar to Eq. (3), concluded that final-state complexity in the electronic wave functions was responsible for Brillouin-zone averaging rather than phonon effects. Our results directly contradict this work, but there are several reasons why this prior study might not have been as sensitive to changes in temperature. First, the maximum Debye-Waller factor differences over the working temperature range were somewhat lower than in our work: 0.33 for Au and 0.35 for Pt, compared to 0.41 for W here. Also, inasmuch as specimen temperatures were not measured directly, it is possible that the lowest temperature was not 77 K, thereby decreasing the change in W. For example, a minimum temperature of 150 K reduces the change in W to only 0.15. Furthermore, the changes in spectra with temperature predicted by the direct-transition model for Au and Pt are not as dramatic as those for W, and thus would, in any case, be more difficult to observe. Finally, it is not clear that the specimen-cleaning treatment left the crystal in an optimally ordered state, as no annealing was performed after a light ion bombardment.

(2) Sayers and McFeely[16] have investigated the problem of phonon involvement in zone averaging in XPS theoretically and have concluded that it is insufficient to account for full averaging. Particularly, they have estimated that, even with multiphonon processes, phonon effects would smear the specification of the *direction* of $\vec{k}^f$ by only ± a few degrees, and, inasmuch as this is still comparable to the typical experimental angular resolution, they conclude that full zone averaging is not possible via this mechanism. However, they appear to neglect the possible three-dimensional character of the phonon smearing on $\vec{k}^f$ which can alter both its *direction* and *magnitude* although energy conservation does limit the smearing in magnitude. Any such three-dimensional smearing is much more effective than the essentially two-dimensional broadening due to the angular resolution. In fact, model calculations we have performed with a sphere of broadening about the final $\vec{k}^f$ value indicate that a sphere with a radius of $0.4(2\pi/a)$ (or the equivalent of a 2.3° direction change), is sufficient to yield a density-of-states-like curve and averaging over ~55% of the Brillouin zone. Shevchik[37] has also recently pointed out that the perturbative analysis utilized by Sayers and McFeely may not be adequate to describe such "intra-atomic" electron-phonon effects. (He also discusses "interatomic" electron-phonon effects that can introduce additional $\vec{k}$ smearing in the final-state wave function, but these are not predicted to be significant in the XPS regime.)

The present study also permits a tentative answer to a question raised by Paasch[17] in connection with the nature of final-state scattering in XPS. He has pointed out that, in the language of diffraction theory, the validity of the direct-transition model as we have used it is equivalent to having a diagonal transmission matrix: That is, neither the bulk or surface potentials induce significant mixing of other plane waves into an initially-excited free-electron-like state at $\vec{k}^f$. The degree of validity of this simple model that we have found for W suggests that the transmission matrix is very nearly diagonal, in spite of the fact that tungsten's high atomic number should make it a strong scatterer of electrons. Part of the explanation of this near-diagonal character no doubt lies in the fact that the individual electron-atom scattering events involved are, at these energies of ~10^3 eV, expected to yield scattered intensity very much peaked in the forward direction, as stressed in recent discussions of core-level XPS angular distributions.[38] Thus, because W is such a strong scatterer, we are led to postulate that such relatively simple direct-transition effects will probably be observable for a broad range of materials, provided that temperatures can be found for which the Debye-Waller factor is sufficiently large. For example, the values in Table I indicate that, even with only liquid-nitrogen cooling, a fairly large number of elements should exhibit a Debye-Waller factor as large as that for W at room temperature. With liquid-helium cooling, an even larger number should exhibit significant direct-transition effects (for example, over $\frac{3}{4}$ of the elements in Table I).

Finally, we note that a further area of interest from a theoretical point of view is obviously to try more-accurate theoretical models which include matrix-element effects as well as $\vec{k}$ conservation in the analysis. For example, such matrix elements might be computed using tight-binding-type wave functions and atomiclike cross sections, as have been used in prior analyses of zone-averaged XPS data.[16,39]

V. CONCLUSIONS

This investigation thus leads to the conclusion that direct transitions can be observed in angle-resolved XPS valence-band spectra provided the Debye-Waller factor is not too small. A simple

direct-transition model based on free-electron final-state dispersion and constant matrix elements for all allowed transitions is also capable of giving a very good first-order description of peak-intensity changes with emission direction. The strong temperature dependence noted in XPS valence-band spectra furthermore strongly suggests that phonon-assisted nondirect transitions are the mechanism for Brillouin-zone averaging and, conversely, that complexities in the final electronic states are not very important. This conclusion thus disagrees with two prior studies by Dabbousi *et al.*[14] and by Sayers and McFeely,[16] for reasons which we have discussed. Temperature-dependent data have further permitted isolating the direct and nondirect components in spectra. Thus, further experiments at lower temperatures to reduce phonon effects, and with better angular resolution to minimize the region in $\vec{k}$-space sampled, could yield relatively straightforward band-structure mapping in the XPS regime of energy. Finally, it thus appears that the free-electron final-state dispersion relation $E^f = \hbar^2(k^f)^2/2m$ is a reasonably accurate approximation for use in analyzing the direct-transition component of angle-resolved photoemission data for metals over the full energy range from ~40 to 1500 eV.

ACKNOWLEDGMENTS

We are indebted to R. E. Connelly for assistance in performing these experiments and also to T. T. Bopp for suggesting the method of analysis represented by Eq. (5). The support of the National Science Foundation (Grant No. CHE76-24506) and the Petroleum Research Fund administered by the American Chemical Society is also gratefully acknowledged.

*Present address: Materials and Molecular Research Division, Lawrence Berkeley Laboratory, University of California, Berkeley, California 94720.
†Present address: Department of Chemistry, University of Utah, Salt Lake City, Utah 84112.

[1]R. J. Baird, C. S. Fadley, and L. F. Wagner, Faraday Discuss. Chem. Soc. 60, 143 (1975); R. J. Baird, L. F. Wagner, and C. S. Fadley, Phys. Rev. Lett. 37, 111 (1976).
[2]F. R. McFeely, J. Stöhr, G. Apai, P. S. Wehner, and D. A. Shirley, Phys. Rev. B 14, 3273 (1976).
[3]L. F. Wagner, Z. Hussain, C. S. Fadley, and R. J. Baird, Solid State Commun. 21, 453 (1977).
[4]G. Apai, J. Stöhr, R. S. Williams, S. P. Kowalczyk, and D. A. Shirley, Phys. Rev. B 15, 584 (1977).
[5]Z. Hussain, L. F. Wagner, and C. S. Fadley, unpublished results for platinum.
[6]N. Erikson, Phys. Scr. 16, 462 (1977).
[7]R. H. Williams, P. C. Kemeny, and L. Ley, Solid State Commun. 21, 453 (1977).
[8]L. F. Wagner, Z. Hussain, and C. S. Fadley, Solid State Commun. 21, 257 (1977).
[9]J. Stöhr, P. S. Wehner, R. S. Williams, G. Apai, and D. A. Shirley, Phys. Rev. B 17, 587 (1978).
[10]R. S. Williams, P. S. Wehner, J. Stöhr, and D. A. Shirley, Phys. Rev. Lett. 39, 302 (1977).
[11]P. Thiry, D. Chandesri, J. Lecante, C. G. Guillot, R. Pinchaux, and Y. Petroff, Phys. Rev. Lett. 73, 82 (1979).
[12]Z. Hussain, S. Kono, L-G. Petersson, C. S. Fadley, and L. F. Wagner, Phys. Rev. B, in press.
[13]Z. Hussain, N. F. T. Hall, L. F. Wagner, S. P. Kowalczyk, C. S. Fadley, K. A. Thomson, and R. L. Dodd, Solid State Commun. 25, 907 (1978).
[14]O. B. Dabbousi, P. S. Wehner, and D. A. Shirley, Solid State Commun. 28, 227 (1978).
[15]P. S. Wehner, J. Stöhr, G. Apai, F. R. McFeely, and D. A. Shirley, Phys. Rev. Lett. 38, 169 (1977).
[16]M. J. Sayers and F. R. McFeely, Phys. Rev. B 17, 3867 (1978).
[17]G. Paasch, Phys. Status Solidi B 87, 191 (1978).
[18]S. Goldberg, C. S. Fadley, and S. Kono, Solid State Commun. 28, 459 (1978).
[19]N. J. Shevchik, J. Phys. C 10, L555 (1977); Phys. Rev. B 16, 3428 (1977).
[20]Z. Hussain, S. Kono, R. E. Connelly, and C. S. Fadley, Phys. Rev. Lett. 44, 895 (1980).
[21]C. S. Fadley in *Electron Spectroscopy: Theory, Techniques, and Applications*, edited by C. R. Brundle and A. D. Baker (Pergamon, 1978), Vol. II, Chap. 1.
[22]J. H. Scofield, J. Electron. Spectrosc. Relat. Phenom. 8, 129 (1976).
[23]R. J. Baird and C. S. Fadley, J. Electron. Spectrosc. Relat. Phenom. 11, 39 (1977).
[24]M. Mehta and C. S. Fadley, Phys. Rev. Lett. 39, 1569 (1977).
[25]A. Savitzky and M. J. E. Golay, Anal. Chem. 36, 1627 (1964); J. A. Steiner, Y. Termonia, and J. Deltour, Anal. Chem. 44, 1906 (1972).
[26]T. M. Duc, G. Guillot, Y. Lassailly, J. Lecante, Y. Jugent, J. C. Verdine, Phys. Rev. Lett. 43, 789 (1979).
[27]N. E. Christensen and B. Feuerbacher, Phys. Rev. B 10, 2349 (1974).
[28]M. L. Tarng and G. K. Wehner, J. Appl. Phys. 44, 1543 (1973).
[29]B. E. Warren, *X-Ray Diffraction* (Addison-Wesley, Reading, Mass., 1969), Chap. 11; J. B. Pendry, *Low-Energy Electron Diffraction* (Academic, New York, 1974).
[30]C. Kittel, *Introduction to Solid State Physics* (Wiley, New York, 1971).
[31]S. Goldberg and C. S. Fadley, J. Electron. Spectrosc. Relat. Phenom., in press.
[32]S. T. Manson and J. W. Cooper, Phys. Rev. 165, 126 (1968).

[33]I. Stansgaard, L. C. Feldman, and P. J. Silverman, Phys. Rev. Lett. 42, 247 (1979); A. J. Melmed, R. T. Tung, W. R. Graham, and G. D. W. Smith, Phys. Rev. Lett. 43, 1521 (1979).
[34]R. J. Reid, Surf. Sci. 29, 623 (1972).
[35]G. E. Laramore and C. B. Duke, Phys. Rev. B 2, 4783 (1970).
[36]J. A. Knapp, F. J. Himpsel, A. R. Williams, and D. A. Eastman, Phys. Rev. B 19, 2844 (1979).
[37]N. J. Shevchik, Phys. Rev. B 20, 3020 (1979).
[38]S. Kono, S. M. Goldberg, N. F. T. Hall, and C. S. Fadley, Phys. Rev. Lett. 41, 1831 (1978); L.-G. Petersson, S. Kono, N. F. T. Hall, C. S. Fadley, and J. B. Pendry, Phys. Rev. Lett. 42, 1545 (1979).
[39]T. Jarlborg and P. O. Nilsson, J. Phys. C 12, 265 (1979).